APPENDIX I

X-RAY DIFFRACTION ANALYSIS RESULTS

INTRODUCTION

Two sandstone and one silstone sample from wells TIBU-469C and Casabe 1045 make up the material of this project.

Sample preparation was carried out in the normal way of clay separation and diffraction analysis and being completed in the Hull University, Geology Departament by Dr. A. Fraser.

SAMPLE PREPARATION

Whole rock powders were mounted in aluminium holdrs prior to analysis. The clay samples were prepared for mounting in a standard series of steps:

1. vigorous agitation in a food blender for 15-20 seconds to achieve as complete disaggregation as possible.

2. extraction of the < 2-3μm fraction by sedimentation.

3. concentration by centrifuging where appropriate, and

4. transferring concentrated slurry onto a glass slide and drying at ambient temperature.

The instrumental conditions employed in the diffractometer runs for the whole rock and clay fraction are indicated on the respective strip chart records. Four runs were made on the clay samples, the two heat treatments being carried out at 335°C, and 575 °C respectively.

RESULTS

Whole rock analysis

The mineral components identified from each of the three samples along with their relative proportions are presented in table 2.

The sample from well TIBU-469C differes significantly from the material of well Casabe-1045 in a number of respects. In particular, the former has a very low total clay fraction, a feldspar content restricted to a modest 4% (+2%) of K-felspar, and finally a major calcite presence, presumably in the form of cement. Chlorite is apparently absent in this sample but the abundance of relatively strongly absorbing calcite could account for the lack of evidence for such a phase.

The calcite reflections are systematically displaced to slightly higher 2θ values relative to the published data, corresponding to a diminution of the d-spacings by an average of 0.01Å. The precise significance of this shift cannot be stated though a small Fe content is one possibility.

An additional difference is the exclusive occurrence of a small amount of halite in the TIBU-469-C sandstone. This is probably a contaminant.

By contrast, the Casabe-1045 samples are richly feldspathic with both plagioclase and K-feldspar represented, they lack carbonate, and have an appreciable mica and clay matrix. Chiorite is detected in trace amounts in the Casabe samples. The clay fraction analysis does not confirm this, but it will be observed that the evidence for Chiorite in the whole rock diffractograms of samples CSB-1045-4078 and CSB-1045-4460 is marginal.

The higher clay and mica content of the CBE-coded samples applies mainly to the mica/illite element. Quantification of this composite component it complicated, principally by the nature and relative mix of the different polytypes. The sum of the intensity ratios of the individual phases for samples CSB-1045-4460 was exceptionally low, therefore normalisation to 100% may well have introduced some distortion of the actual mineral proportions. The mica/illite component is likely to be affected most by any distorting factor. As a rough check, the < 4μm fraction, from which the final clay fraction was extracted, was weighed and compared with the weight of the residue. The fine fractions was found to be approximately 15% of the total rock by weight, a result which indicates that the mica/illite and kaolinite values are moderately correct if somewhat low. The mica/illite content probably corresponds to the uppermost value of the range quoted, ie. 10%.

The clay component of sample CSB-1045-4460 is also notable for the conspicous low angle tail on the kaolinite 001 reflection at ~12.5°C, and the strong suggestion of subsidiary peak at approximately 11.9°C. There is a prime case here for positiong halloysite (the 7Å-type, structurally bonded H_2O layer). Sample CSB-1045-4078

displays a comparable though less well marked feature which points to a similar conclusion.

Only a few, more minor, points on the whole rock mmineralogy remain to be mentioned. The plagioclase is sodic in composition, and, on the bases of the angular position of the 060 reflection at -41.8°C, the K-feldspar is dominantly, if not wholly, triclinic (microcline).

Clay fraction analysis

As with the whole rock data, the results of the clay analysis presented in table 2 bring out significant differences between the two wells, although it is noteworthy that there are important common factors throughout, such as the dominance of kaolinite and the presence of minor chlorite.

Each of the diffraction traces has a distinctive nature and for this reason, discussion of the clay fraction will be given on a individual samples basis.

Sample TIBU-469C-616.6: has a straightforward diffraction pattern which stems from the presence of three single clay species of which kaolinite greatly predominates whilst the subsidiary illite and chlorite are represented equally. No expanding or interstratified components were detected from either the glycolated or the first healt-treted material.

Sample CSB-1045-4078: has air dry and glycolated traces which are closey similar in pattern to those of sample, CSB-1045-4460, the only appreciable difference being evident in the region between 4° 2θ and 8° 2θ where the 15Å peak on the air dry run shifts to a 16.8Å peak on glycol solvation. The angular positions and low intensities of the peaks concerned denote only a minor amount of pure smectite. This conclusion is confirmed by the small degree of intensification of the 10Å reflection at 8.9° 2θ after heating. Again, to judge mainly from the low angle tail on the 7Å line profile, there seems to be fairly clear evidence of halloysite and this is consistent with the whole rock data. Chlorite is more evidently present CBE-1045-4460 as shown by the 001 reflection; nevertheless, as in sample CBE-1045-4460, the occurrence of a tail rather than a distinc shoulder on the high angle side of the 3.6Å. profile renders quantification uncertain. The halloysite contribution to the chlorite value quoted i table 2 has not been evaluated.

When the sample set is viewed as a whole, the dominance of kaolinite stands out as the most salient feature. Smectite is limited to well CBE-1045. There are an insufficient number of samples to establish any trends or patterns of variation.

Sample CSB-1045-4060: yielded a complex diffractogram. The innermost reflection (ie. the one with lowest 2θ) on the air dry run shows a fairly intense peak centred on 2θ=5.9 , the d-spacing for which is almost exactly 15Å. The 10Å illite reflection at around 8.8° 2θ is a relatively small but clearly defined one located on the high angle limb of the strong 15Å line profile. Another strong reflection has its maximum intensity at

12.35°2θ, the d-spacing of 7.17A coinciding exactly with kaolinite 001. However, in both the run at 1 2θ/min and in the re-run at 0.5 2θ/min, but especially in the latter case, the profile obviously lacks perfect symmetry in having a poronunced low angle tail and even the suggestion of an actual shoulder at 11.85°2θ (d=7.54A). Similary, the 002 reflection just below 25°2θ displays asymmetry, though in this case it results from a high angle tail. Although interpretation cannot be completely certain, ;the feactures mentioned concerniing the subsidiary peak position and profile characteristics correspond exactly to the 7Å species of halloysite. The evidence from the whole rock data is thus confirmed. Quantification has not been attempeted but the halloysite is probably very subordinate to the kaolinite. Because the form of the asymmetry in the 3.6Å reflection results in overlap with the chlorite 004 reflections, the ahalloysite is more reably included with the chlorite (Table 2).

After glycolation the 7Å and 10Å peaks remain the same, excep that the latter hecomes more clearly defined in relation to the background. A conspicous shift of the 5.9°2 θ (15Å) reflection to 5.3 20 has taken place following expansion of the basal spacing to 16.7A. Higher order reflections of the same basal planes occur at about 10.7 20 (d=8.3Å) and 16.6°2θ (d=5.5Å) though in both cases, the profiles tend to be rather broad and asymmetric. A smectite species insfirmaly indicated, which, if glycolation is asumed to have gone to completion, is interlayered with approximately 15%-20% chlorite.

Inspection of the diffraction traces generated from the heat-treated material of this sample appears to cast some doubt on the above conclusion regadirng smectite. Very unexpectedly, the first heating at 350°C yieds a very broad peak centred on 6.3 2θ the d-spacing for which is 14Å. Identical results were obteined fromtwo separately prepared samples so that the effect of the heating must be regarded as authentic. Such behaviour strongly suggest a swelling chlorite rather than smectite but, to confound matters still further, the second heat treatment at 575°C leaves an almost negligible chlorite 001 reflection at about 6.5°2θ. At the same time, a very considerable intensification of the 10Å reflection occurs together with the develoment of a porminent low angle tail on the profile. The strengthened 10Å reflection tallies with a collapsed structure and, in the absence of any previous experience of swelling chlorite on the part of the present operator, the evidence is taken to favour the original diagnosis of smectite. The low angle tail lends excellent support to a modest degree of chlorite interstratification. The anomaluous response to the first heat treatments cannot be explained satisfactorily and speculations is not attempted here.

As shown in table 2, a normal chlorite is believed to be present at the very minor level of 5%+2%. It is necessary to re-iterate however, that identification of chlorite and computing its amounts are bases primarily on the high angle tail of the 3.6A reflection near 25°2θ. If the particular asymmetry of the profile is largely the result of halloysite, as suggested earlier, then the chlorite component will require to be reduced accordingly. In fact, the very weak reflection after heating at 575°C indicates only a trace amount of chlorite.

Plate 1-1 TS photomicrograph showing a fine to very fine grained, moderately well to well sorted (visually estimated), lithic arenite. This sandstone has a good primary and secondary macropore system, in its lower part, in which the principal control on permeability is likely to be the degree of constriction of pore throats by compaction. Note that in the upper part of the photomicrograph (B) the pore system is seriously degraded by compaction of ductile grains.

Sample CSB 1045-4252, well Casabe 1045, depth 4252.0ft.
$\emptyset_{He}$ = 18.9%, K_h = 38.0mD, Ømacro = 13.1%.
Scale bar is 250µm across, plain-polarised light. →

Plate 1-2 SEI photomicrograph illustrating a fine to medium-grained (visually estimated) arenite with a good macropore system. Note that grains are poorly rounded and display no evidence of modification by authigenic phases.

Sample CSB 1045-4252, well Casabe 1045, depth 4252.0ft.
$\emptyset_{He}$ = 18.9%, K_h = 38.0mD, Ømacro = 13.1%.
Scale bar is 200µm across, secondary electron image. →


B
A


124X 20KV WD:15MM S:00000 P:00009
200UM

Plate 1-3 TS photomicrograph of a coarse silt to very fine sand grade, moderately well sorted (visually estimated) subfeldspathic wacke. The siltstone is essentially non-porous but has discontinuous coarser grained laminae (a) with primary macropore systems.

Sample CSB 1045-4460, well Casabe 1045, depth 4460.0ft.
$\varnothing_{He}$ = NA, K_h = NA, Ømacro = trace.
Scale bar is 250µm across, plain-polarised light. →

Plate 1-4 SEI photomicrograph of a coarse-silt to very fine sand grade wacke with interparticle areas plugged by detrital clay. Macropores are isolated and will not form an effective pore system.

Sample CSB 1045-4460, well Casabe 1045, depth 4460.0ft.
$\varnothing_{He}$ = NA, K_h = NA, Ømacro = trace.
Scale bar is 200µm across, secondary electron image. →

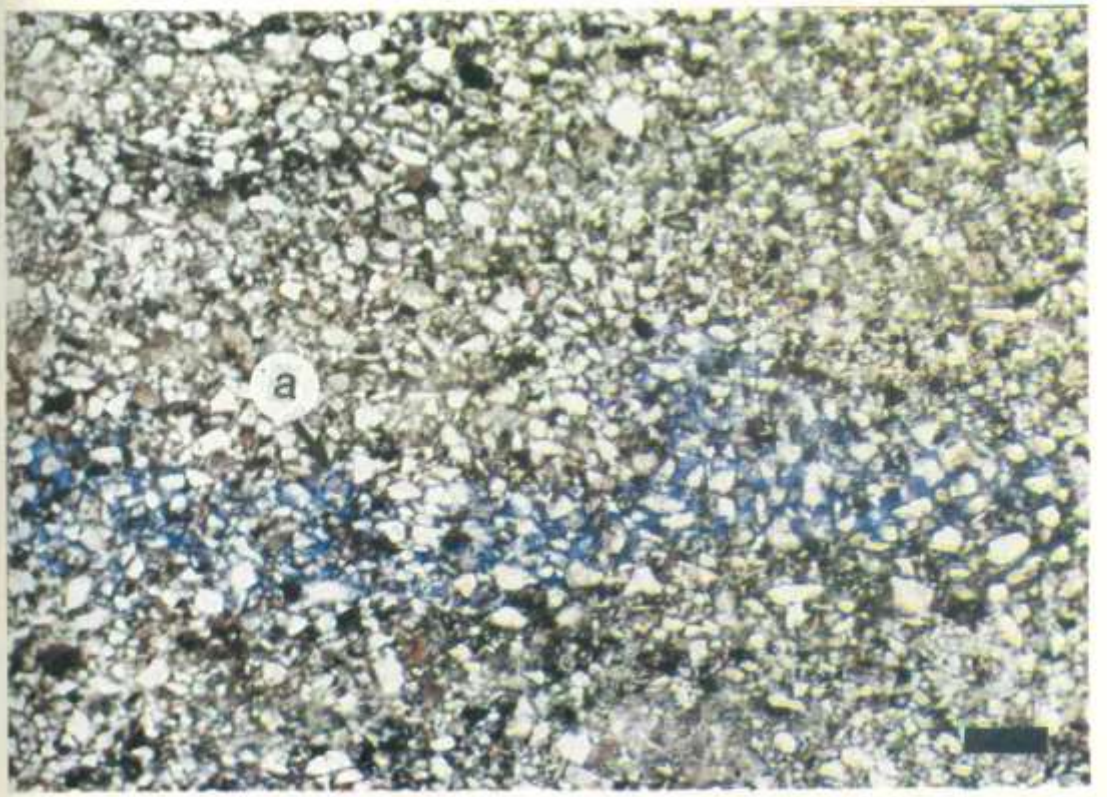
a


226X 20KV WD:18MM S:00000 P:00000
200UM

Plate 2-1 TS photomicrograph of a fine to medium-grained, moderately-sorted sandstone (visually estimated) of lithic composition. The ductile deformation of lithic fragments (a) has effectively destroyed the initial macropore system in this part of the sandstone. The comparison of Plates 2-1 and 2-2 illustrates the mm-scale variability in pore system in this sandstone.

Sample CSB 1045-4087, well Casabe 1045, depth 4252.0ft.
$\emptyset_{He}$ = 26.9%, K_h = 167.0mD, Ømacro = 9.5%.
Scale bar is 250µm across, plain-polarised light. →

Plate 2-2 BEI photomicrograph of a fine to medium-grained, moderate to moderately well sorted sandstone (visually estimated). Note that the sandstone has a macropore network (a) but deformation of ductile and unstable brittle grains (b) has extensively destroyed this system.

Sample CSB 1045-4089, well Casabe 1045, depth 4089.0ft.
$\emptyset_{He}$ = 27.9%, K_h = 227.0mD, Ømacro = NM
Scale bar is 1000µm across, backscatter electron image. →

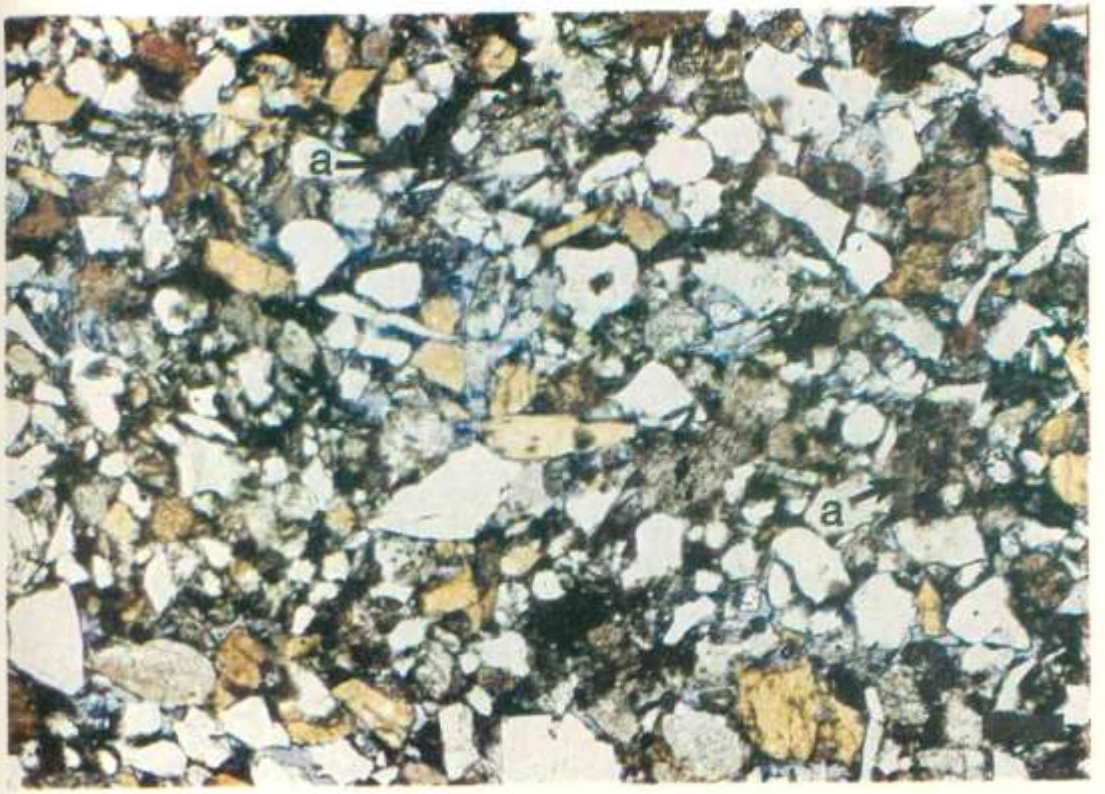
a
a


46,8X 20KV WD:25MM S:04089 P:00002
1MM
b
b
a
a

Plate 2-3 TS photomicrograph of a medium to coarse grained, moderately well to well sorted (visually estimated), lithic arenite. The sandstone is cemented by feroan calcite (a) which has destroyed the initial pore system of the sandstone. Note the collapse structure in partially dissolved K-feldspar (b) and the grain fracture (c) which occurred prior to ferroan calcite cementation.

Sample CSB 1045-4252, well Casabe 1045, depth 4252.0ft.
$\emptyset_{He}$ = 18.9%, K_h = 38.0mD, Ømacro = 13.1%.
Scale bar is 250µm across, plain-polarised light. →

Plate 3-1 BEI photomicrograph of a splayed and plastically deformed mica (a). Note that splayed mica flakes block pore throats (b) and destroy primary macroporosity (c). Splayed portions of the mica are less bright (d) indicating incipient kaolinitisation of the grain.

Sample CSB 1045-4089, well Casabe 1045, depth 4089.0ft.
$\emptyset_{He}$ = 27.9%, K_h = 227.0mD, Ømacro = NM.
Scale bar is 100µm across, backscatter electron image. →

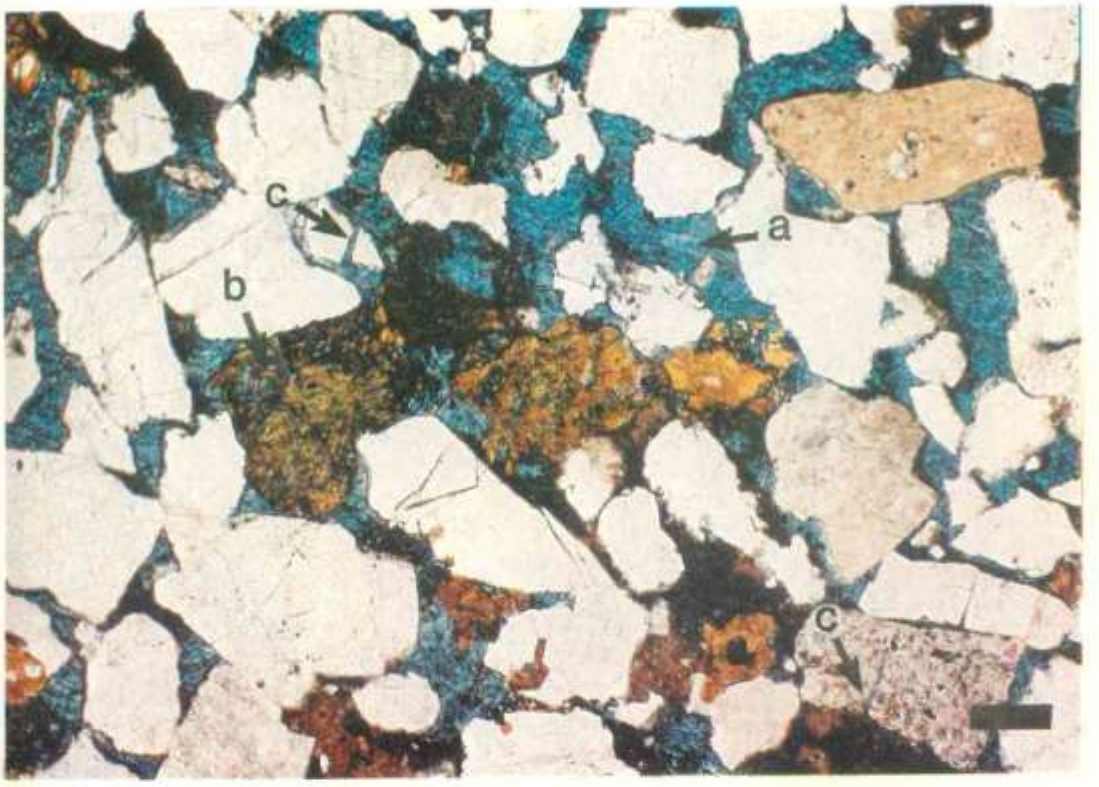
c
a
b
c

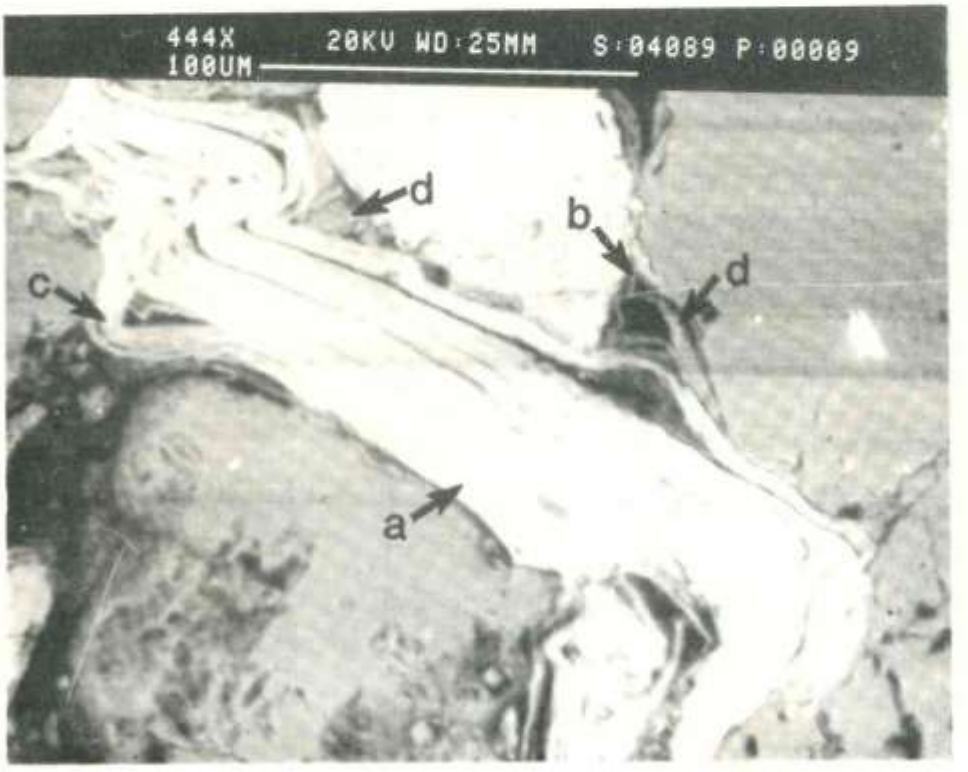
444X 20KV WD:25MM S:04089 P:00009
100UM
d
b
d
c
a

Plate 3-2 BEI photomicrograph showing a splayed mica (a). Note that the splaying of the mica has closed pore throats (b) and will reduce interconnectivity between macropores. K-feldspar grains have undergone partial dissolution and grain collapse (c).

Sample CSB 1045-4089, well Casabe 1045, depth 4089.0ft.
$Ø_{He}$ = 27.9%, K_h = 227.0mD, Ømacro = NM.
Scale bar is 200µm across, backscatter electron image. →

Plate 3-3 TS photomicrograph illustrating a mudclast (a), which has deformed plastically causing the destruction of primary porosity and the blockage of pore throats (b). Note that adjacent quartz grains are fractured and that the fractures are filled with ferroan calcite (c).

Sample Tibu-469-616.5, well Tibu 469C, depth 616.5ft.
$Ø_{He}$ = NA, K_h = NA, Ømacro = 0.5%.
Scale bar is 100µm across, plain-polarised light. →


152X 20KV WD:25MM S:04089 P:00004
200UM
b
a
c

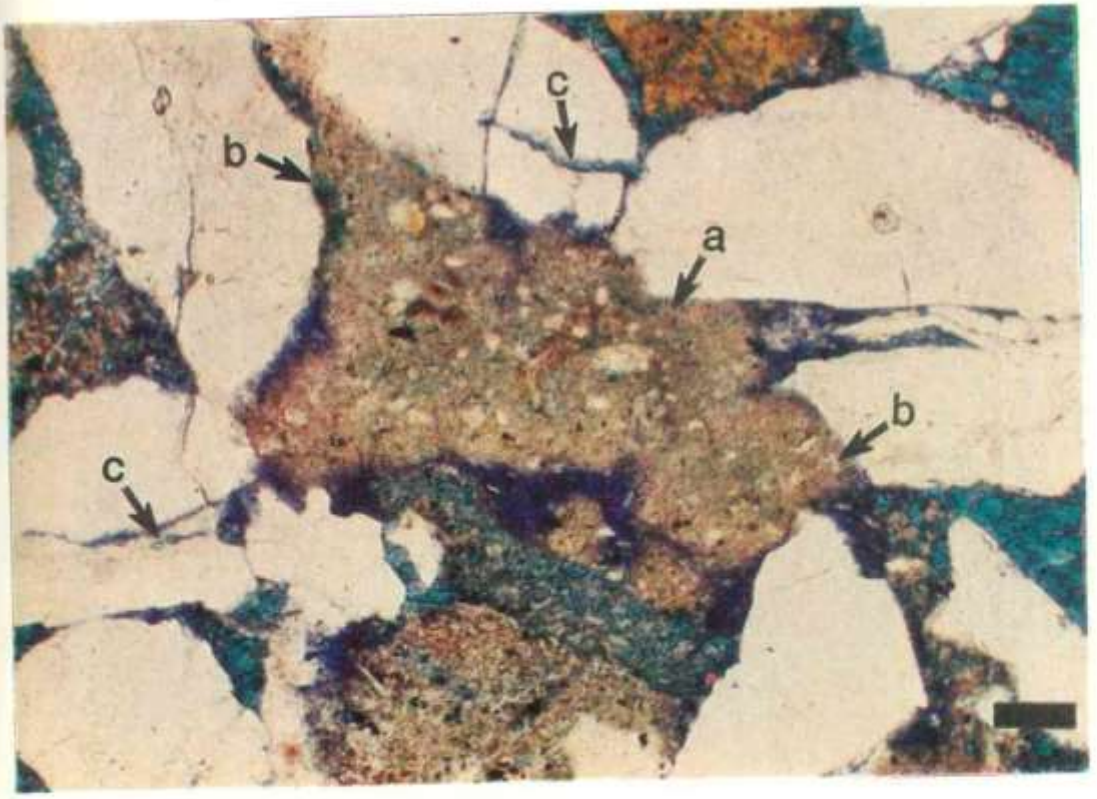
c
b
a
b
c

Plate 4-1 TS photomicrograph of spherulitic siderite lining a pore (a). Note that the siderite has been partially dissolved (b) and corroded (c) prior to cementation by ferroan calcite (d). Note the ferroan calcite filled fracture (e) and the pyrite framboid engulfed by ferroan calcite (f).

Sample Tibu-469-616.5, well Tibu-469C, depth 616.5ft.
$\emptyset_{He}$ = NA, K_h = NA, Ømacro = 0.5%.
Scale bar is 50µm across, plain-polarised light. →

Plate 4-2 SEI photomicrograph of poorly crystalline kaolinite booklets lining a pore (a). Note that the pores also contain minor detrital clay (b), but are otherwise clean. Migration of isolated kaolinite booklets or individual kaolinite platelets under adverse flow conditions could result in the blockage of pore throats and decrease in permeability.

Sample CSB 1045-4460, well Casabe 1045, depth 4460.0ft.
$\emptyset_{He}$ = 18.9%, K_h = 38.0mD, Ømacro = 13.1%.
Scale bar is 20µm across, secondary electron image. →

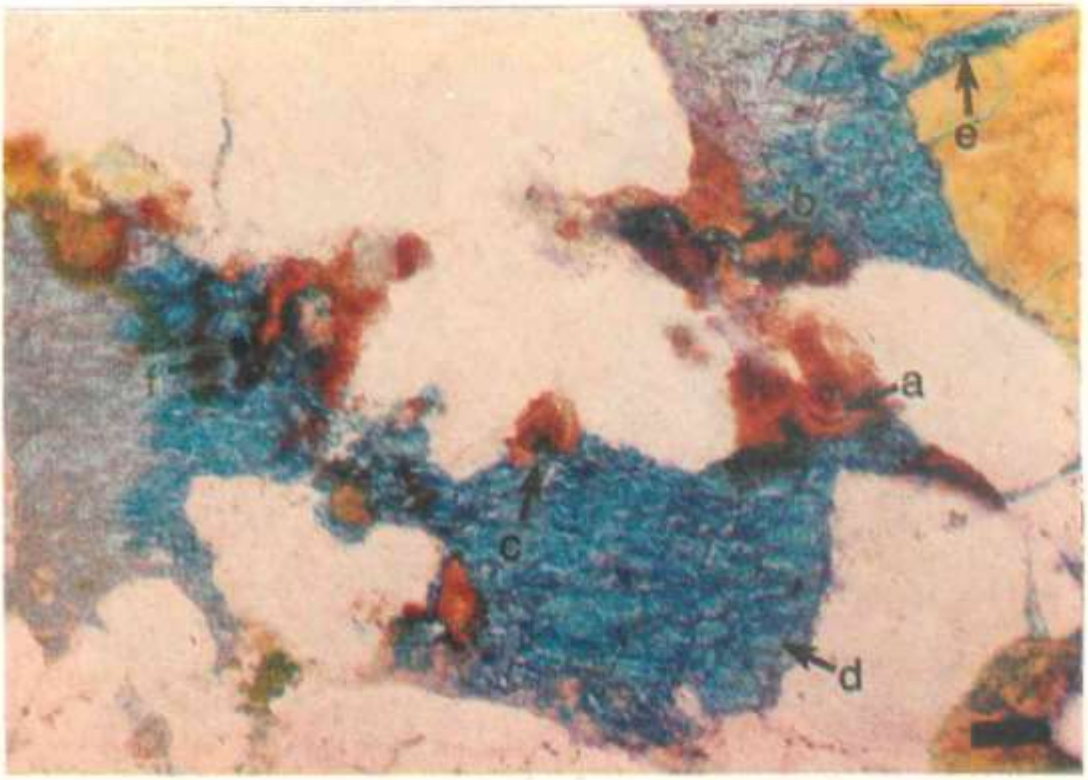
e
b
a
f
c
d


1,84KX 20KV WD:17MM S:84460 P:00002
20UM
b
a

Plate 4-3 SEI photomicrograph of crystalline kaolinite booklets (a) plugging a pore throat. Note that the grain surfaces are otherwise free of clay.

Sample CSB 1045-4252, well Casabe 1045, depth 4252.0ft.
$\emptyset_{He}$ = 18.9%, K_h = 38.0mD, Ømacro = 13.1%.
Scale bar is 50µm across, secondary electron image. →

Plate 5-1 TS photomicrograph of an extensively dissolved K-feldspar (a), with anatase precipitated in the dissolution pore (b) prior to ferroan calcite cementation (c) and primary and secondary porosity destruction. Note the scattered pyrite framboids enveloped by the ferroan calcite (d).

Sample Tibu-469-616.5, well Tibu-469C, depth 616.5ft..
$\emptyset_{He}$ = NA, K_h = NA, Ømacro = 0.5%.
Scale bar is 50µm across, plain-polarised light. →


1,00KX 20KV WD:15MM S:04252 P:00010
50UM
a

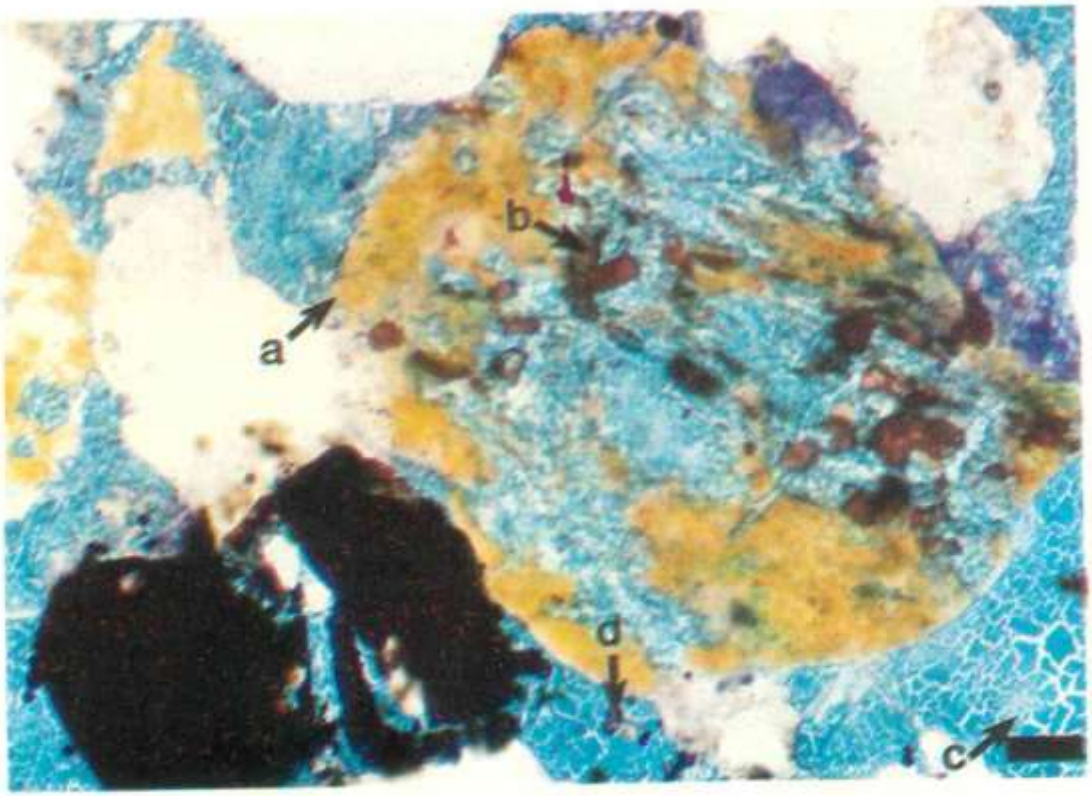
a
b
d
c

Plate 5-2 TS photomicrograph illustrating ferroan calcite (a) which locally fills pores. This form of ferroan calcite will not significantly affect permeability in this reservoir sandstone.

Sample CSB 1045-4252, well Casabe 1045, depth 4252.0ft.
$\varnothing_{He}$ = 18.9%, K_h = 38.0mD, Ømacro = 13.1%.
Scale bar is 100μm across, plain-polarised light. →

Plate 5-3 BEI photomicrograph showing pore filling ferroan calcite (a) destroying primary porosity (b). Note that ferroan calcite also replaces grains (c), probably feldspar. Ferroan calcite post-dates grain contact dissolution which has caused coarse, elongate grain contacts (d).

Sample CSB 1045-4206, well Casabe 1045, depth 4206.0ft.
$\varnothing_{He}$ = 31.9%, K_h = 709.0mD, Ømacro = NM.
Scale bar is 200μm across, backscatter electron image. →

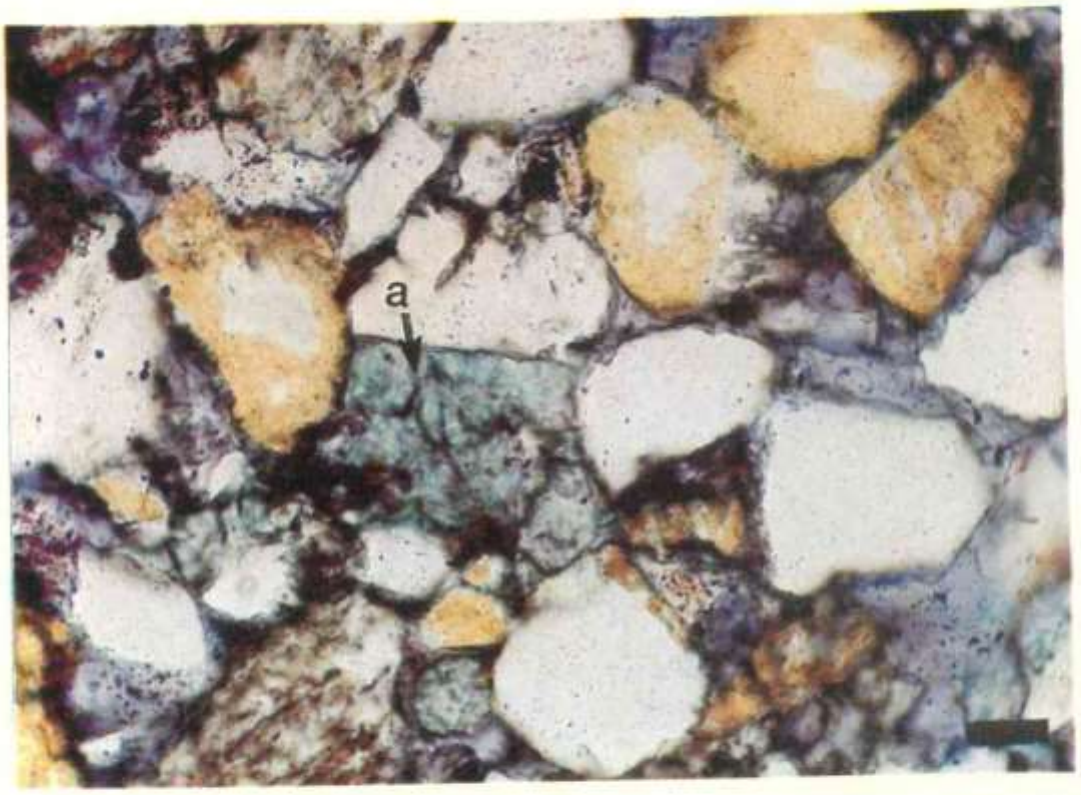
a


161X 20KV WD:24MM S:04206 P:00011
200UM
d
a
b
c

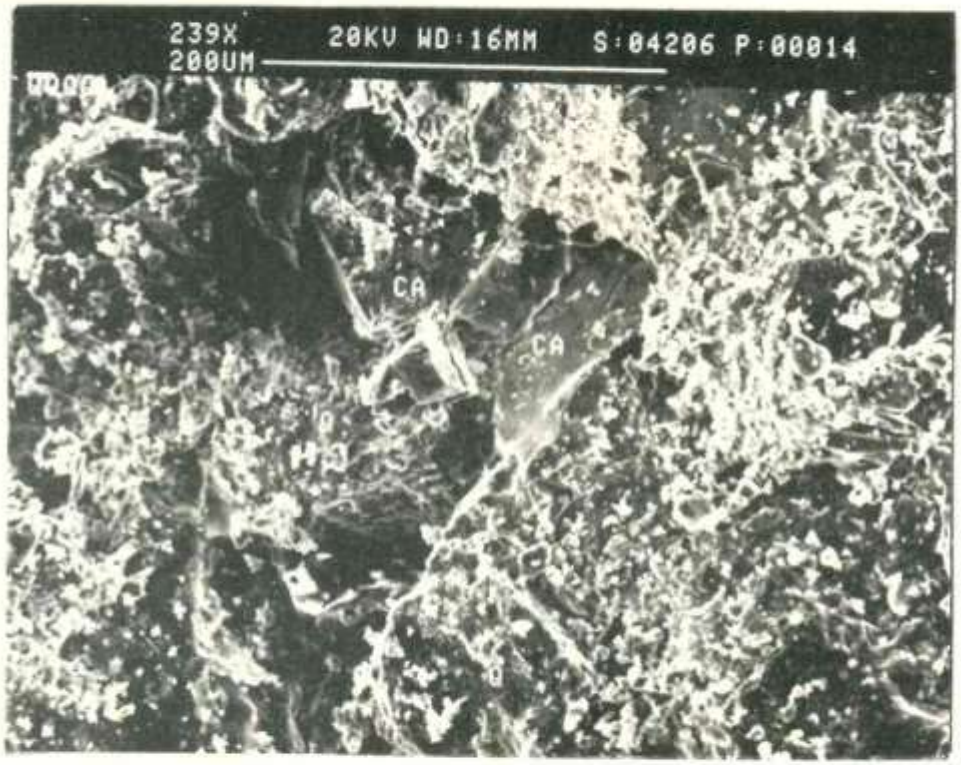

Plate 5-4 SEI photomicrograph of calcite (Ca) partially filling a pore and blocking pore throats. Note that the framework quartz grains (Q) do not have overgrowths and pores are generally clean.

Sample CSB 1045-4206, well Casabe 1045, depth 4206.0ft.
$Ø_{He}$ = 31.9%, K_h = 709.0mD, Ømacro = NM.
Scale bar is 200µm across, secondary electron image.